Dynamic association of the ULK1 complex with omegasomes during autophagy induction

Eleftherios Karanasios[1], Eloise Stapleton[1,*], Maria Manifava[1], Takeshi Kaizuka[2,3], Noboru Mizushima[2,3], Simon A. Walker[1] and Nicholas T. Ktistakis[1,‡]

[1]Signalling Programme, The Babraham Institute, Babraham, Cambridge CB22 3AT,
[2]Department of Biochemistry and Molecular Biology, Graduate School and Faculty of Medicine, The University of Tokyo, Tokyo 113-0033, Japan
[3]Department of Physiology and Cell Biology, Tokyo Medical and Dental University, Tokyo 113-8519, Japan

*Present address: MRC Group, Cardiff School of Biosciences, Cardiff University, Cardiff CF10 3AX, UK
‡Author for correspondence (nicholas.ktistakis@babraham.ac.uk)

Accepted 27 August 2013
Journal of Cell Science 126, 5224–5238

doi: 10.1242/jcs.132415

Summary

Induction of autophagy requires the ULK1 protein kinase complex and the Vps34 lipid kinase complex. PtdIns3*P* synthesised by Vps34 accumulates in omegasomes, membrane extensions of the ER within which some autophagosomes form. The ULK1 complex is thought to target autophagosomes independently of PtdIns3*P*, and its functional relationship to omegasomes is unclear. Here we show that the ULK1 complex colocalises with omegasomes in a PtdIns3*P*-dependent way. Live-cell imaging of Atg13 (a ULK1 complex component), omegasomes and LC3 establishes and annotates for the first time a complete sequence of steps leading to autophagosome formation, as follows. Upon starvation, the ULK1 complex forms puncta associated with the ER and sporadically with mitochondria. If PtdIns3*P* is available, these puncta become omegasomes. Subsequently, the ULK1 complex exits omegasomes and autophagosomes bud off. If PtdIns3*P* is unavailable, ULK1 puncta are greatly reduced in number and duration. Atg13 contains a region with affinity for acidic phospholipids, required for translocation to punctate structures and autophagy progression.

Key words: ULK complex, Autophagy, Imaging, Omegasomes, Phosphatidylinositol 3-phosphate

Introduction

Autophagy is a membrane trafficking pathway to lysosomes employed by all cells to recycle nutrients under periods of starvation, or to degrade protein aggregates and damaged or superfluous organelles and pathogens (Mizushima and Komatsu, 2011; Rabinowitz and White, 2010). The autophagic programme is activated by a variety of factors, such as amino acid limitation, low cellular energy, changes in pH or temperature, hypoxia, oxidative stress, pathogen infection and removal of growth factors (Burman and Ktistakis, 2010; Yang and Klionsky, 2010). It is well established that autophagy is crucial for the homeostasis of both cells and tissues, and its dysfunction causes disease, with most notable involvement in neurodegeneration, cancer and ageing (Mizushima and Komatsu, 2011; Sridhar et al., 2012).

A hallmark of autophagy is the formation of autophagosomes, double membrane vesicles that appear *de novo* and enclose cargo originating from the cytoplasm. The proteins that constitute the core autophagic machinery are well known and conserved from yeast to mammals (Inoue and Klionsky, 2010; Suzuki and Ohsumi, 2010) but the origin and mechanism of formation of the double membrane autophagosomes are still under investigation.

In terms of mechanism, the core autophagic machinery is organized in functional complexes that act in a coordinated fashion for the formation of autophagosomes (reviewed by Mizushima and Komatsu, 2011; Mizushima et al., 2011; Rubinsztein et al., 2012). When nutrients become sparse, the ULK1 complex is no longer repressed by the mTORC1 [mechanistic (or mammalian) target of rapamycin complex 1] kinase and translocates to membranes (this is known as the initiation stage), where it activates the Vps34 complex thus stimulating the local synthesis of phosphatidylinositol 3-phosphate (PtdIns3*P*; the nucleation stage). In some settings at least, the presence of PtdIns3*P* leads to formation of omegasomes (Axe et al., 2008), which are membrane platforms connected to the endoplasmic reticulum (ER). At the omegasome membrane, several downstream components are recruited, leading to the expansion of the autophagosomal membrane (the elongation stage). These components include vesicles containing the Atg9 protein, which interact with omegasomes without fusing with them, and two conjugation systems, leading ultimately to the covalent modification of LC3 with phosphatidylethanolamine (PE). LC3 is the major protein of mature autophagosomes and it aids expansion as well as closure of the autophagosomal membrane (the fusion stage). The origin of the autophagosomal membrane appears to be variable (Rubinsztein et al., 2012; Tooze and Yoshimori, 2010). For omegasome-related events that are preceded by ULK1 complex activation, most evidence points to the ER (Hayashi-Nishino et al., 2009; Ylä-Anttila et al., 2009). Alternative locales, including the mitochondria, the plasma membrane and the Golgi apparatus, have also been reported (Bodemann et al., 2011; Geng et al., 2010; Hailey et al., 2010; Ravikumar et al., 2010).

Omegasomes aid in autophagosome biogenesis in two ways. In addition to attracting down-stream effectors, some of which are direct targets of PtdIns3*P* [e.g. members of the WIPI family of proteins (Lu et al., 2011; Polson et al., 2010; Proikas-Cezanne

et al., 2004)], omegasomes also physically demarcate the outer edges of the growing autophagosomal membrane until those edges fuse to generate the double membrane vesicle. However, the connection of omegasomes to upstream components such as the ULK1 complex is not clear. Although downregulation of proteins of the ULK1 complex inhibits the formation of omegasomes, inhibition of Vps34 has been reported not to prevent the starvation-induced translocation of ULK1 to puncta (Itakura and Mizushima, 2010; Orsi et al., 2012). At the same time, components of the ULK1 complex and omegasomes have been reported to be close but physically distinct during autophagy (Itakura and Mizushima, 2010), suggesting that the ULK1 complex may leave the pre-autophagosomal sites before omegasomes are formed.

The aim of this work was to determine the interaction of the ULK1 complex with omegasomes in HEK293 cells. We found that the ULK1 complex becomes part of omegasomes in a PtdIns3*P*-dependent way, but leaves those sites before the autophagosomal budding step. We show and annotate for the first time a complete sequence of steps leading to autophagosome formation and the proximity of the earliest discernible structures to various cellular membranes. Finally, we present evidence that Atg13, a member of the ULK1 complex, contains a membrane-binding site that is important for the translocation of the complex to early autophagosomal structures.

Results

Endogenous proteins of the ULK1 complex target a compartment closely associated with omegasomes

The current model suggests that, during autophagy, the activated ULK1 complex translocates to ER, on sites that are close but distinct from omegasomes, where it stimulates PtdIns3*P* synthesis and drives the recruitment of PtdIns3*P* effectors such as DFCP1 and the WIPIs (Mizushima and Komatsu, 2011). This model predicts that the ULK1 complex translocates to the ER before omegasomes are formed and remains spatially adjacent to omegasomes. In order to examine this model in a human cell line, we established the localization of endogenous proteins of the ULK1 complex in HEK293 cells stably expressing the omegasome marker GFP–DFCP1 (Axe et al., 2008). We found that in starved cells, 80% of omegasomes colocalised with punctate structures formed of ULK1, Atg13 and Atg101 (three of the four proteins of the ULK1 complex) (Fig. 1A). Ring-shaped omegasomes associated at the centre of their ring with puncta decorated with ULK1, Atg13 and Atg101 (arrows in Fig. 1A), whereas non-ring-shaped omegasomes overlapped partially (arrowheads in Fig. 1A) with the ULK1 complex. A population of smaller diameter ULK1, Atg13 and Atg101 puncta did not associate with omegasomes, but we note that many such puncta were also present in non-starved cells (see control ULK1 staining in Fig. 1A). We concluded that, during starvation, the ULK1 complex translocates to puncta, which are often spatially connected to omegasomes.

The translocation of the ULK1 complex to starvation-induced puncta is responsive to PtdIns3*P* levels

The ULK1 complex stimulates PtdIns3*P* synthesis, which must be sustained for the formation of omegasomes (Di Bartolomeo et al., 2010), and the puncta associated with the ULK1 complex (hereafter referred to as ULK1 puncta) also associate with omegasomes, which are PtdIns3*P*-rich structures. Thus we hypothesized that the translocation of the ULK1 complex to starvation-induced puncta might be responsive to PtdIns3*P* levels. To test this, we examined whether in the parental HEK293 cells the translocation of endogenous ULK1, Atg13 and Atg101 to puncta under autophagy-inducing conditions is disrupted by wortmannin, which is an inhibitor of the class III phosphatidylinositol 3-kinase (Fig. 1B). As a positive control we used WIPI2, a well characterised PtdIns3*P* effector in this pathway (Polson et al., 2010). We found that in the absence of wortmannin, induction of autophagy by either starvation or the mTOR inhibitor PP242, increased the number of WIPI2 puncta per cell by more than sixfold compared with control conditions (Fig. 1B). Addition of wortmannin reduced WIPI2 puncta to levels similar to those in the control conditions (Fig. 1B). Similarly, under normal conditions the number of ULK1 puncta per cell was 2.1 ± 1 and induction of autophagy, either by starvation or by PP242, increased them by approximately fourfold (Fig. 1B). Inhibition of PtdIns3*P* synthesis decreased the number of ULK1 puncta per cell to levels similar to the control (Fig. 1B). The same wortmannin sensitivity was seen for the other two proteins of the ULK1 complex, Atg13 and Atg101 (Fig. 1B). As it was previously shown (Axe et al., 2008), addition of wortmannin almost abolished the formation of omegasomes; under those conditions the wortmannin-resistant Atg13 puncta were largely free of omegasome components (supplementary material Fig. S1A). Finally, depletion of the Vps34 complex member Beclin1 markedly reduced the number of large puncta that were formed under starvation by the endogenous Atg13 (supplementary material Fig. S1B,C). In summary, PtdIns3*P* synthesis affects the targeting of the ULK1 complex to starvation-induced puncta.

GFP–Atg13 localization pattern is representative of the ULK1 complex

The colocalization between omegasomes and the ULK1 complex reported above suggests a dynamic relationship between the two. To explore this further by live-cell imaging, we established a clonal cell line stably expressing GFP–Atg13. Atg13 is a well characterised member of the ULK1 complex (Chang and Neufeld, 2009; Ganley et al., 2009; Hosokawa et al., 2009; Jung et al., 2009). We favoured it over the other proteins of the complex because it is conserved from yeast to mammals (unlike Atg101), it does not have additional functions (unlike FIP200) and it does not appear to inhibit autophagy upon overexpression (unlike ULK1). During starvation, GFP–Atg13 was recruited to puncta, whose number increased with time (supplementary material Fig. S2A and Movie 1) and colocalised completely with puncta of the endogenous ULK1 and Atg101 (supplementary material Fig. S2B,C), as well as with puncta of the early autophagy markers WIPI2 and Atg16 (supplementary material Fig. S2B). Finally, the formation of GFP–Atg13 puncta was inhibited by wortmannin treatment (supplementary material Fig. S2B). Thus the localization of the exogenously expressed GFP–Atg13 followed the pattern of the endogenous ULK1 complex, hence justifying its further use for functional analysis. To ensure that downstream autophagy response was unaffected in these cells, we used western blotting to examine the conversion of LC3-I to LC3-II, a commonly used biochemical assay for autophagy (Klionsky et al., 2012). The two clones mostly used in this work (clone13 and clone35) had the same starvation response as the parental HEK293 cells (supplementary material Fig. S2D).

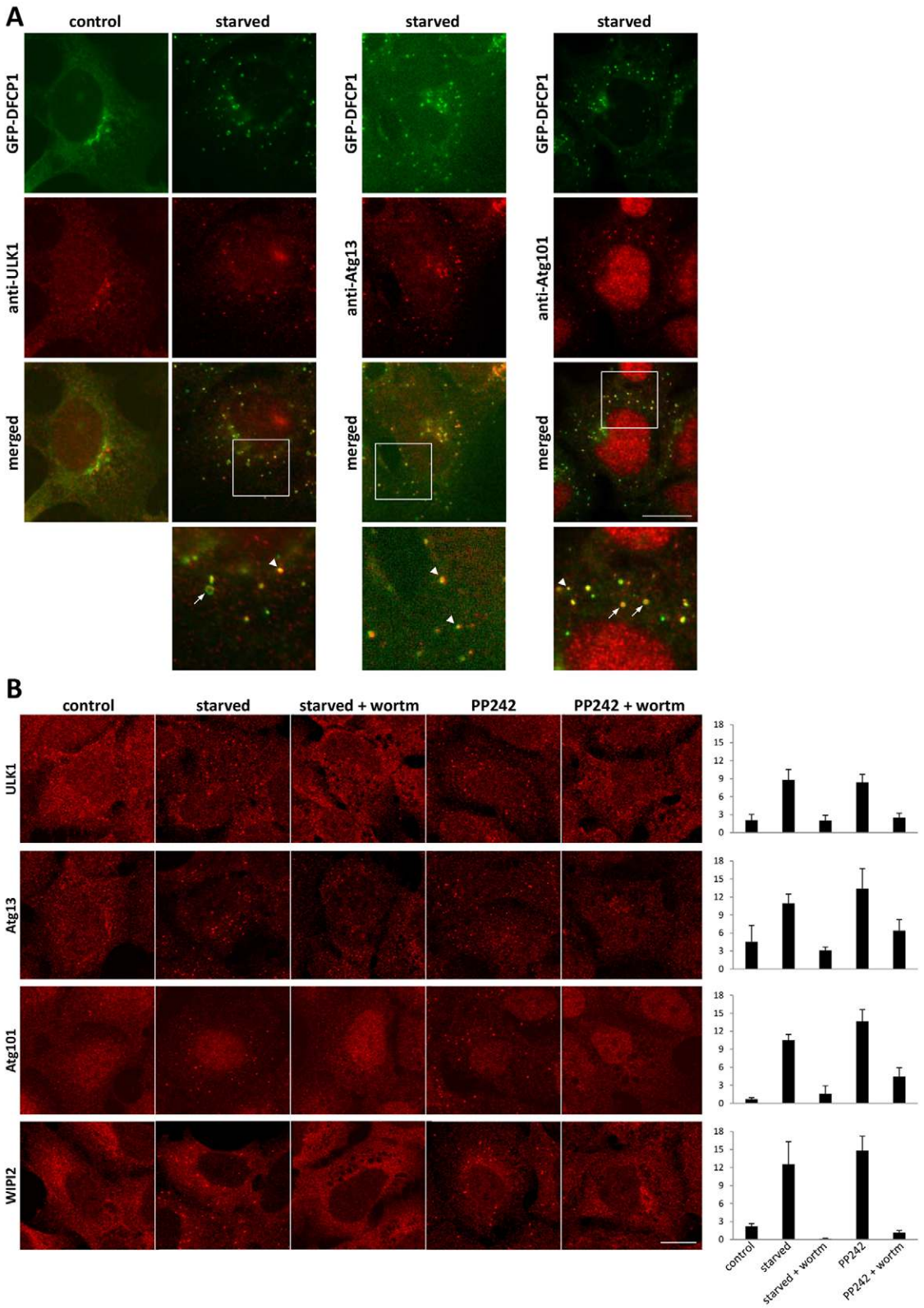

Fig. 1. The ULK1 complex translocates to PtdIns3*P*-sensitive puncta during autophagy. (A) HEK293 cells stably expressing GFP–DFCP1 were starved for 1 hour, fixed and stained with antibodies against ULK1, Atg13 and Atg101. Representative images are shown. Arrowheads point to small omegasomes tangential with particles from the ULK1 complex. Arrows point to ring-shaped omegasomes, which associate in the middle with particles from the ULK1 complex. (B) HEK293 cells were starved or treated with PP242 for 1 hour, in the absence or presence of wortmannin, and immunolabelled for endogenous ULK1, Atg13, Atg101 and WIPI2. Representative confocal images are shown. Puncta were counted using Imaris. Values are means ± s.d. puncta per cell, for at least 10 different fields with 15–30 cells each. Scale bars: ~10 μm.

PtdIns3*P* synthesis affects the size and lifespan of Atg13 puncta

We next wanted to examine the dynamics of Atg13 translocation to puncta under starvation and correlate them with PtdIns3*P* synthesis by employing the PI 3-kinase inhibitor wortmannin. We found that addition of wortmannin to starved cells dramatically reduced the total amount of GFP–Atg13 puncta after just a few minutes, without completely abolishing them (Fig. 2A,B; supplementary material Movie 2). The pre-existing puncta continued their lifecycle until they collapsed, while new, smaller puncta formed at a much slower rate. The effect of wortmannin on the number of Atg13 puncta might be explained if PtdIns3*P* synthesis creates a positive feedback loop that reinforces the translocation of Atg13 to puncta, therefore increasing their lifespan. To test this, we quantified the lifespan of Atg13 puncta, from the moment that they emerge until they collapse, both in the absence and presence of wortmannin. We found that the lifespan of Atg13 puncta follows a near normal distribution, and the addition of wortmannin shortens their average lifespan by more than twofold (201 and 86 seconds, respectively; Fig. 2D,E). Moreover, the size of Atg13 puncta that continued to form in the presence of wortmannin and the total amount of Atg13 recruited on those structures were significantly reduced compared with those formed under normal starvation (Fig. 2C,F,G). A similar trend was also observed for endogenous Atg101 in fixed cells (Fig. 2H,I). We concluded that Atg13 puncta require sustained PtdIns3*P* synthesis in order to reach their maximum size and lifespan.

Relationship of Atg13 puncta to ER and mitochondria

The origin of the autophagosomal membrane remains an unresolved conundrum of the autophagy field, with ER, mitochondria and plasma membrane being the main candidates (Rubinsztein et al., 2012; Tooze and Yoshimori, 2010). Part of the uncertainty is probably related to the variability of the experimental settings under which autophagy is induced. A second confounding factor is the extremely dynamic nature of autophagosomes, which allows them to appear in close proximity to many membranes. Earlier work using exogenous ULK1 indicated that starvation-induced puncta of this protein are seen in association with the ER and frequently move with the ER strands (Itakura and Mizushima, 2010). Here we re-examined this question but used Atg13, and considered only newly formed puncta that were clearly distinguishable by spinning disk confocal microscopy. In addition, because wortmannin reduces the size and lifespan of Atg13 puncta without completely blocking their formation, we postulated that particles forming in the presence of this drug might represent the earliest visible intermediate of forming autophagosomes. When comparing the spatial relationship of GFP–Atg13 puncta with ER, mitochondria and lysosomes (Fig. 3B) we found that, in the absence of wortmannin, the Atg13 particles were always formed in close association with ER (Fig. 3A example 1, D), frequently but not always close to mitochondria (Fig. 3A examples 2 and 3, D) and less frequently in the vicinity of lysosomes (Fig. 3D). Importantly, the association between the emerging Atg13 particles and ER, mitochondria and lysosomes in the presence of wortmannin was not altered (Fig. 3D,E). The spatial relationship between Atg13 puncta and ER was also examined by super resolution microscopy, which showed that the Atg13 particles are well-defined structures that associate tightly with but are distinct from the strands of ER (Fig. 3F). Taking everything into account we concluded that Atg13 puncta form in tight association with ER, and that inhibition of PtdIns3*P* synthesis does not alter their subcellular localization. Thus PtdIns3*P* is not the signal that targets Atg13 to ER, and targeting to the ER under starvation conditions in the absence of PtdIns3*P* is not sufficient to allow Atg13 (and by extension the ULK1 complex) to fulfil its membrane-associated cycle.

Dynamic association of Atg13 with expanding omegasomes

It is clear from our data that PtdIns3*P* synthesis enhances the number, size and lifetime of the ULK1 particles. Given the fact that omegasomes represent a PtdIns3*P* platform for early autophagy events, it was of special interest to determine how they engage with Atg13 puncta. We used live-cell imaging in cells stably expressing GFP–DFCP1 and mCherry–Atg13. We found that throughout starvation mCherry–Atg13 puncta colocalised with omegasomes (Fig. 4A; supplementary material Movie 3), in agreement with the localization of the endogenous Atg13 (Fig. 1). Only one Atg13 punctum associated with each omegasome, and a typical sequence is shown in Fig. 4B; supplementary material Movie 4. Once the two particles formed (Fig. 4B yellow and white arrows) they expanded together. The omegasome often developed the hallmark ring shape, whereas Atg13 remained as a punctate structure enlarging to fill the interior of the omegasome. Interestingly, the Atg13 puncta did not stay on omegasomes throughout the lifetime of the latter: in the example shown in Fig. 4B, the Atg13 punctum started to disappear after about 3 minutes, while the omegasome was still visible (blue arrows). After the Atg13 signal disappeared, the omegasome underwent a characteristic transformation whereby its membrane elongated, suggestive of a ‘budding’ step [Fig. 4B blue arrows (see also Axe et al., 2008)]. At the end of this sequence the omegasome collapsed and largely disappeared (Fig. 4B last three frames). A schematic representation of this sequence is shown in Fig. 4C: the green line represents the duration of the GFP–DFCP1 structure, the red line the equivalent for mCherry–Atg13, and the blue symbol marks the budding stage. To determine the order of recruitment of Atg13 and DFCP1 and their respective dynamics, examples from more than 10 videos were analysed as described in Fig. 4C, always choosing events clearly starting *de novo*. In total, we analysed 45 such events, which are depicted in supplementary material Fig. S3. The temporal relationship between Atg13 and DFCP1 puncta was slightly variable at the beginning but similar for the subsequent steps. At the beginning of the sequence the relative occurrence of the visible Atg13 and omegasome puncta was variable or hard to determine. In the majority of events, Atg13-positive puncta and omegasomes formed nearly simultaneously or within half a minute of each other, but in some events, either the Atg13 punctum or the omegasomes had a clear precedence (supplementary material Fig. S3). Once formed, the Atg13 and DFCP1 mixed membrane expanded, typically for 2 minutes, before Atg13 disappeared. Importantly, the budding step took place almost always after the Atg13 had left the omegasome (there were only few exceptions shown for the 45 events analysed in supplementary material Fig. S3), most typically within 1 minute from the disappearance of Atg13, and was followed by the diminution and the eventual collapse of the omegasome.

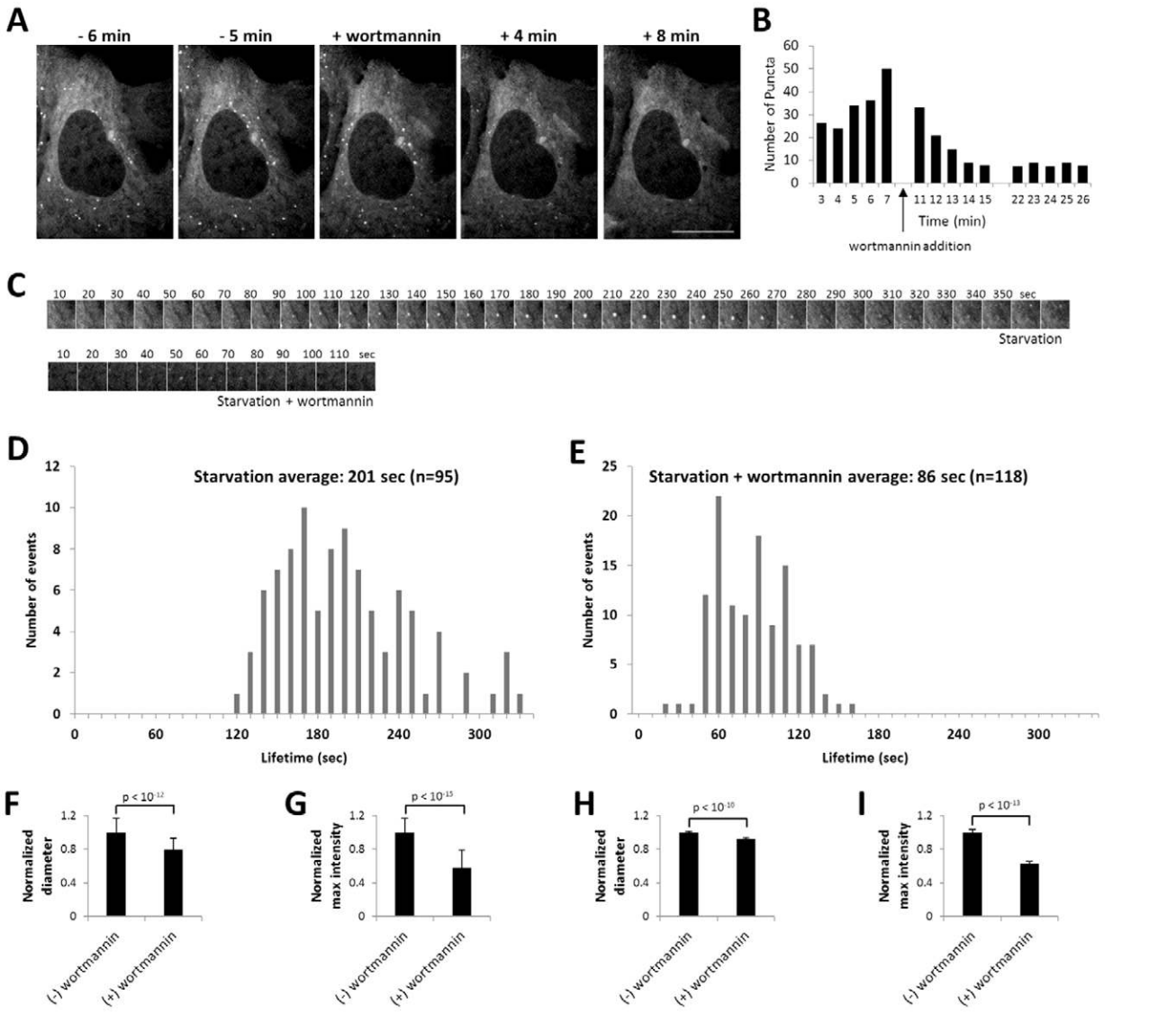

Fig. 2. PtdIns3*P* synthesis reinforces the translocation of Atg13 to puncta under starvation. (A) Live-cell imaging of starved HEK293 cells stably expressing GFP–Atg13 before and after the addition of wortmannin. Representative frames are shown. (B) Number of GFP–Atg13 puncta per field over time, for one field. The arrow marks the addition of wortmannin. (C) Representative images of GFP–Atg13 puncta from emergence to collapse, in the absence or presence of wortmannin. (D,E) The spread of the lifespan of GFP–Atg13 puncta in the absence (D) or presence (E) of wortmannin. Events are defined as independent Atg13 particles formed, from their emergence until their collapse. (F,G) The maximum size of Atg13 puncta was quantified in the absence (67 events from D) or presence of wortmannin (95 events from E). In brief, lines were drawn through the centre of Atg13 particles using ImageJ, the intensity of pixels along the line was plotted and the borders of Atg13 particle were defined as the pixels with fluorescence intensity above the background. Values are means ± s.d. of the diameter (F) and the ratio of maximum to background fluorescence intensity (G) of the Atg13 particles normalized to the values in the absence of wortmannin. (H,I) The maximum size of Atg101 puncta was quantified in the absence or presence of wortmannin (spots from Fig. 1B) using the Spot Detection function of Imaris software (Bitplane). Values are means ± s.d. of the diameter (H) and the maximum fluorescence intensity (I) normalized to values in the absence of wortmannin. Scale bar: ~10 μm.

Autophagosomes are formed following an ordered course of intermediate steps

In a previous study, we showed that each omegasome is the precursor structure that leads to the formation of one LC3-positive autophagosome (Axe et al., 2008), whereas in this study, we have demonstrated that each Atg13 particle associates with one forming omegasome. Taking into consideration both studies, we assumed that autophagosome formation should comprise a reproducible course of events, starting with the nucleation of ULK1 complex and ending with the budding of a mature autophagosome from the omegasome. To show this, we followed, in starved HEK293 cells, the localization of mCherry–Atg13, GFP–DFCP1 and CFP–LC3, in order to capture the spatial and temporal dynamics between the ULK1 complex, omegasomes and LC3, along the course of autophagosome formation. We found that throughout starvation, Atg13 puncta associated with both DFCP1- and LC3-positive structures (Fig. 4D, arrows; supplementary material Movie 5). As predicted, one Atg13 particle associated with only one omegasome and gave rise to a single autophagosome; a typical sequence is shown in Fig. 4E; in

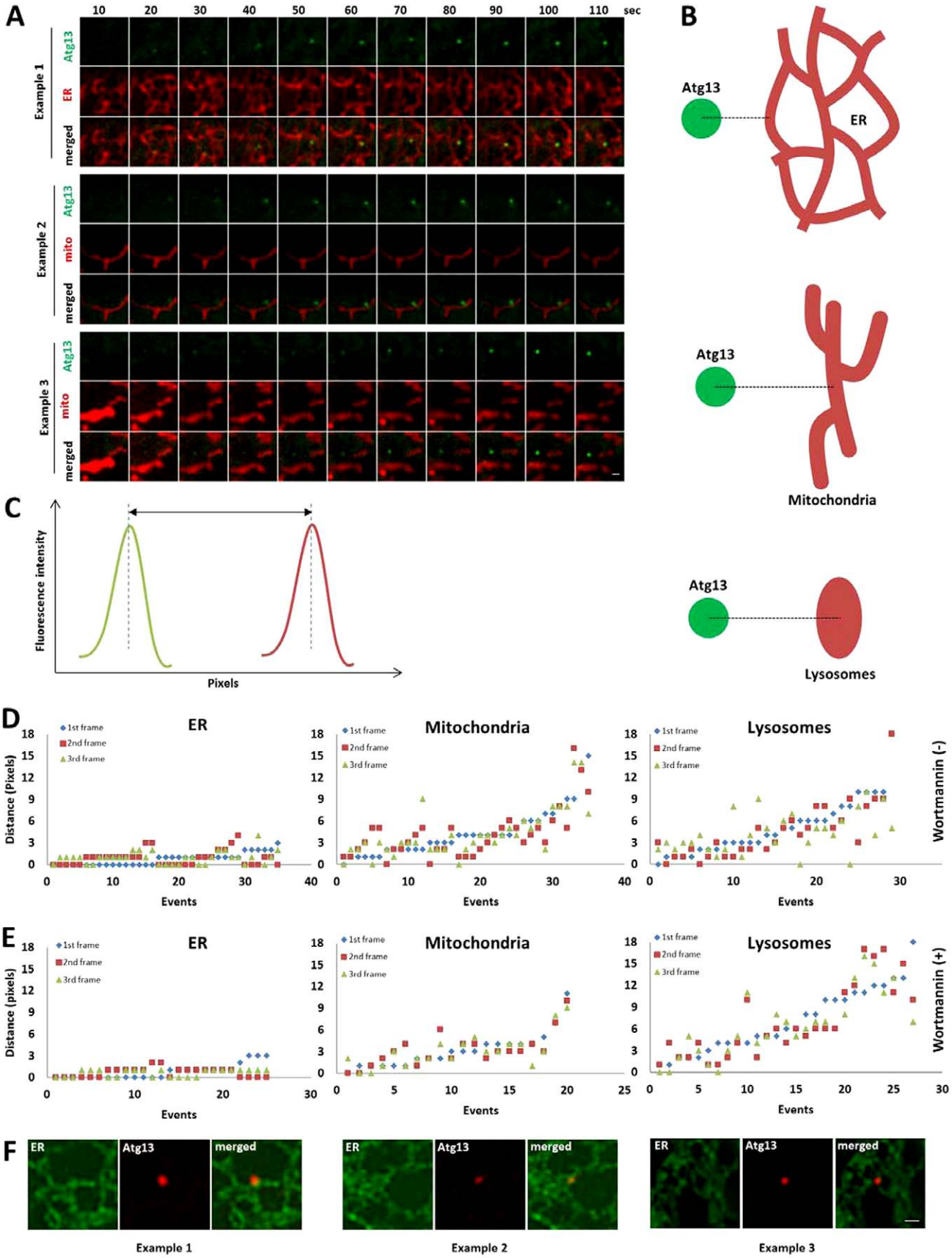

Fig. 3. See next page for legend.

supplementary material Movie 6, example 1. The Atg13 punctum formed and expanded in parallel with the omegasome (Fig. 4E, white arrowheads at 40 seconds), whereas LC3 started to accumulate on the membrane enclosed by the omegasome ring approximately half a minute later (Fig. 4E, yellow arrowheads at 1 minute 10 seconds). The structure marked by the three proteins expanded with them, with the omegasome always enclosing the Atg13- and LC3-positive puncta (Fig. 4E, arrowheads at 3 minutes 20 seconds for a typical snapshot). After about 5 minutes, the Atg13 particle rapidly disappeared, and only omegasome and LC3 staining remained visible (Fig. 4E, arrows at 5 minutes 50 seconds). Within 1 minute of the exit of Atg13, the LC3-containing autophagosome began to bud off from the omegasome (Fig. 4E, arrows at 7 minutes 10 seconds) and shortly thereafter the omegasome staining disappeared, leaving behind only the LC3-containing autophagosome. This sequence verifies that the disappearance of Atg13 from the common membrane precedes the budding step whereby the autophagosome exits the omegasome. In general, this complicated sequence of events, captured here for the first time, shows a remarkable consistency in its timing characteristics. Supplementary material Fig. S4 shows a compressed course for the event just described alongside a different event captured from a different part of the cell and at a different interval during starvation (supplementary material Fig. S4, example A and example B and Movie 6). The sequence of events and their timing is fairly reproducible. Based on the live-cell imaging experiments, we concluded that sustained PtdIns3*P* synthesis induces the expansion of the Atg13-positive nucleation site, and initiates a reproducible course of events that leads to the formation of an autophagosome through an omegasome intermediate.

A site on Atg13 is important for lipid binding and translocation to autophagic puncta

The inhibitory effect of wortmannin on the translocation of Atg13 to puncta, and the tight association of Atg13 particles with the expanding omegasomes, indicated that the localization of Atg13 to early autophagy structures might depend on some lipid affinity. To test this, we scanned the primary sequence of Atg13 for potential domains that could interact with acidic phospholipids, and identified a cluster of one arginine and three lysine residues very near the N-terminus that is conserved in higher eukaryotes (Fig. 5A). When we simultaneously mutated all four residues into alanines, the mutant showed a reduction of 50% in number of GFP–Atg13 puncta during starvation in a mixed stable clone (Fig. 5B,C), whereas the reduction was closer to 75% for single clones derived from this mixed population (Fig. 5D,E). Moreover, the (reduced) number of GFP–Atg13 puncta formed by the mutant clones in the presence of wortmannin was further reduced compared with the wild-type (wt) clones (Fig. 5F). These results suggest that these residues play an important role in the translocation of Atg13 particles to autophagic puncta. Other sites mutagenized on the basis of potential phosphorylation or interaction sites as indicated in Fig. 5A did not interfere with punctum formation and were not considered further (data not shown).

Using a panel of chemically synthesised lipids covalently coupled to a solid support, which we have extensively characterised and validated in our lab (Conway et al., 2010; Delon et al., 2004; Krugmann et al., 2002; Manifava et al., 2001; Ridley et al., 2001), we tested lysates from the clonal cell line expressing the wt GFP–Atg13 for binding to PtdIns3*P*, PtdIns4*P*, PtdIns(3,4)P_2, PtdIns(3,5)P_2, PtdIns(3,4,5)P_3, phosphatidic acid (PA), diacylglycerol (DAG), cardiolipin and sphingosine. Under conditions where endogenous Atg16 did not bind to any of the beads tested, Atg13 bound to PA-, PtdIns3*P*- and PtdIns4*P*-coated beads and more weakly to those coated with PtdIns(3,4,5)P_3 (Fig. 5G). Mutant Atg13 showed decreased affinity for PA by 60% and for PtdIns3*P* and PtdIns4*P* by 80% (Fig. 5H,I). To examine whether these mutations compromise the association of Atg13 with the ULK1 complex, we immunoprecipitated the exact same lysates of wt and mutant GFP–Atg13 shown in Fig. 5H (note that input for H and J are identical and simply duplicated) with antibodies to GFP, and blotted for Atg101 and ULK1. We found that both wt and mutant Atg13 bound to endogenous Atg101 similarly (Fig. 5J), and the same was true for binding to endogenous ULK1 (Fig. 5J). We note that, in our conditions, binding of Atg13 to endogenous Atg101 is almost stoichiometric, whereas binding to endogenous ULK1 is less so. Thus, the mutations of Atg13 did not alter its interaction with Atg101 or ULK1. To compare lipid binding of the mutant with the wt Atg13 in a simpler system, we prepared the two recombinant proteins from bacteria (Fig. 5K) and examined whether they bind to PA, PtdIns3*P* and PtdIns4*P*. The recombinant wt Atg13 bound to the same phospholipids as the GFP–Atg13 from HEK293 lysates (Fig. 5L) but its affinity for PA was stronger than its affinity for PtdIns3*P*, whereas the affinity for PtdIns4*P* was even weaker (Fig. 5L; note that the lipid beads for this experiment were identical to those used in the one shown in Fig. 5H). In agreement with our hypothesis, the mutations of the recombinant Atg13 reduced substantially its affinity for all three phospholipids (Fig. 5L). We concluded that Atg13 has modest affinity for three acidic phospholipids, namely PA, PtdIns3*P* and PtdIns4*P*, which may facilitate its translocation to puncta during starvation.

Because the mutations of Atg13 compromise its binding to lipids without affecting its interaction with the other proteins of

Fig. 3. Relationship of Atg13 puncta to ER, mitochondria and lysosomes. (A) HEK293 cells stably expressing GFP–Atg13 were first either transfected for 24 hours with mCherry-dgk1 (ER reporter; ER) or mRFP-LAMP1 (lysosomes reporter; not shown), or incubated with Mitotracker Red (mito) for 30 minutes, and then starved and imaged. Representative montages of forming GFP–Atg13 puncta close to ER (example 1) close to mitochondria (example 2) or away from mitochondria (example 3) are shown. (B,C) Schematic representation of quantitative analysis of the association between GFP–Atg13 puncta and ER, mitochondria or lysosomes. Lines were drawn to connect the centre of an Atg13 punctum with the closest strand of ER, a mitochondrion or a lysosome (B), the intensities of pixels along the line for both the green and the red channel were plotted, and the distance in pixels between the peaks of the two channels was measured (C). (D,E) Distance, in pixels, between Atg13 spots and ER, mitochondria or lysosomes, for the first three frames from their emergence, in the absence (D) or presence of wortmannin (E). Events are defined as independent Atg13 particles formed, from their emergence until their collapse. For example, for D-ER, we measured 35 unique Atg13 particles emerging *de novo*, and plotted the distance of each to the ER strands for the first three frames. The ordering of the events in the graph is arbitrary and starts from those closest to the ER to those away from the ER. (F) HEK293 cells stably expressing GFP–Atg13 were transfected with mCherry-dgk1 for 24 hours, starved and subjected to structured illumination microscopy (SIM). Three representative examples are shown. Signals from the green and red channel are inversely pseudocoloured as red and green, correspondingly, to allow better visual appreciation of the ER. Scale bars: ~1 μm.

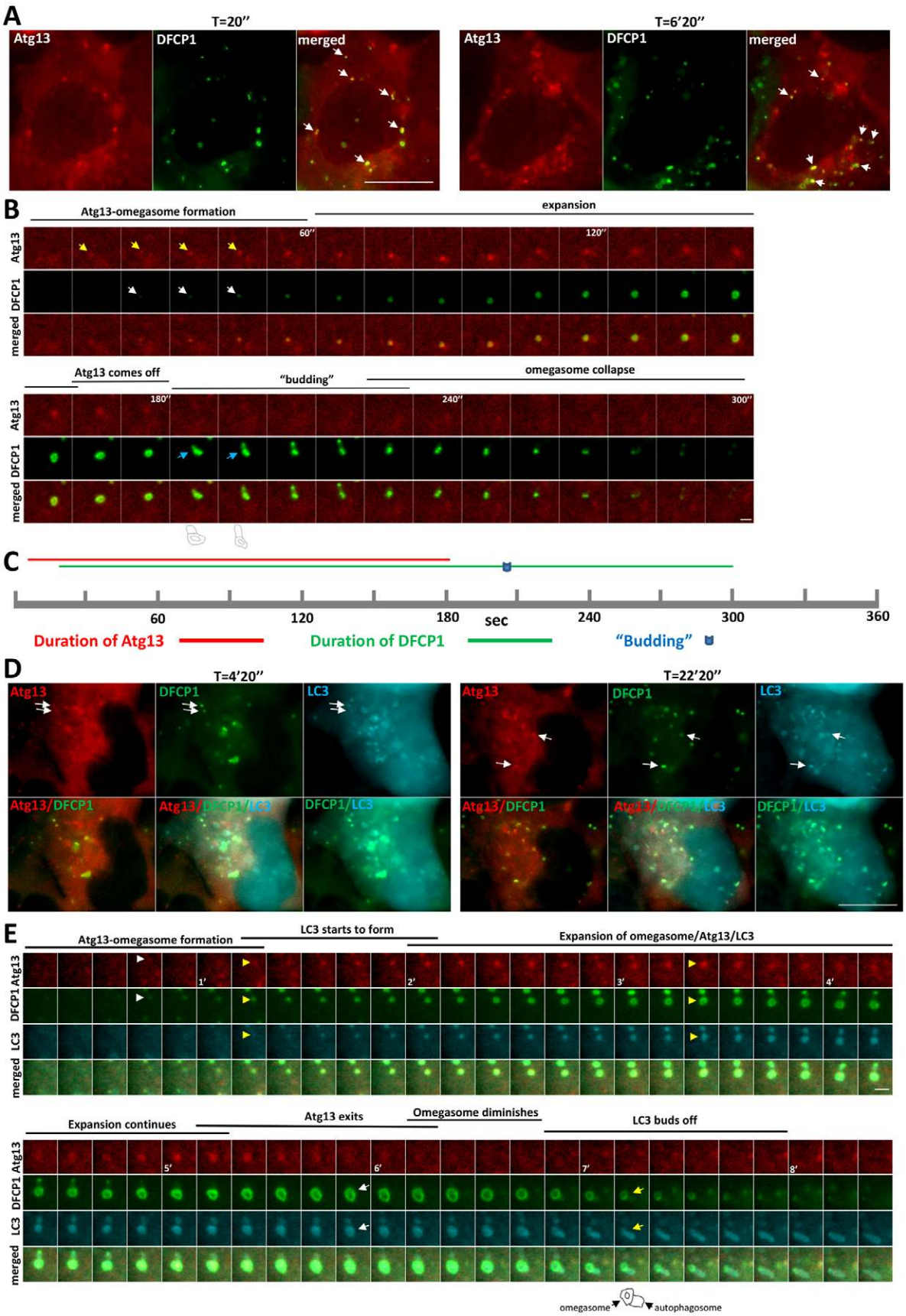

Fig. 4. See next page for legend.

the ULK1 complex, we asked whether the mutant Atg13 has a dominant-negative effect on the autophagy response. In preliminary experiments we noted that in a stable population of mixed clones, expression of the mutant GFP–Atg13 reduced the translocation of endogenous Atg101 to starvation-induced puncta, whereas the wt GFP–Atg13 did not (Fig. 6A). In a stable population of mixed clones or in clones derived from this population, the expression of mutant Atg13 reduced the translocation of endogenous ULK1, Atg101, WIPI2 and Atg16 to puncta by ~50% (Fig. 6B,C). Moreover, stable expression of the mutant GFP–Atg13 in Atg13 knockout MEFs failed to rescue the formation of starvation-induced puncta by the endogenous early autophagy markers WIPI2 and Atg16, whereas expression of wt GFP–Atg13 did (Fig. 6D and supplementary material Fig. S5). We concluded that the positively charged residues at the N-terminus of Atg13 are important for the downstream formation of autophagic puncta.

Discussion

Translocation of the ULK1 complex to early autophagic structures, including omegasomes, is stabilised by sustained PtdIns3*P* synthesis

We have found that when HEK293 cells are treated with wortmannin under autophagy-inducing conditions, the number of puncta formed by the ULK1 complex decreases. At the same time, live imaging experiments using GFP–Atg13 as a proxy for the ULK1 complex, show that wortmannin reduces the number of newly formed autophagic puncta, and those few that form have a much shorter lifespan. Thus, PtdIns3*P* synthesis is important for the recruitment of the ULK1 complex to autophagic puncta, and for its stabilization on these structures. This is very consistent with another of our findings, namely that the ULK1 complex becomes part of the omegasome structure, a signature membrane for PtdIns3*P* synthesis during autophagy.

Our findings that, in the absence of PtdIns3*P* synthesis, some ULK1 complex is recruited to puncta, are in broad agreement with a previous study of mouse embryonic fibroblasts (Itakura and Mizushima, 2010), and are consistent with the idea that translocation of ULK1 to a pre-autophagosomal membrane, most probably the ER, is a pre-requisite for the subsequent activation of the Vps34 complex (Di Bartolomeo et al., 2010; Matsunaga et al., 2010). It is possible that newly formed PtdIns3*P* may create a positive feedback loop, which reinforces the recruitment of the ULK1 complex, further stimulating PtdIns3*P* synthesis. This interplay between translocation of the ULK1 complex and PtdIns3*P* synthesis would be very rapid and may be the reason why we could not establish that during normal autophagy the formation of ULK1 puncta clearly precedes omegasome emergence. A recent study has shown that during autophagosome formation, Atg14, which is the autophagy-specific component of the Vps34 complex, translocates to the ER–mitochondria contact points (Hamasaki et al., 2013); the formation of these contact points is necessary for the correct localization of Atg14. An intriguing possibility is that PtdIns3*P* synthesis stabilizes the ER–mitochondria contact points, which feed back to the ULK1 complex and promote autophagosome formation.

Fig. 4. Atg13 colocalises with omegasomes but separates before the autophagosomal budding step. (A) Live-cell imaging of starved HEK293 cells stably expressing GFP–DFCP1 and mCherry–Atg13. Two representative frames of different time points are shown. Arrows point to Atg13 particles that colocalise with omegasomes. (B) Representative montage showing the spatial and temporal relationship between one Atg13 particle and one omegasome. Frames were captured every 10 seconds. Yellow arrows indicate the emergence of the Atg13 particle. White arrows indicate the emergence of the omegasome. Blue arrows indicate membrane budding off the omegasome ring. (C) Schematic illustration of the temporal relationship shown in B, paralleling the lifespan of an Atg13 particle with the formation, budding and collapse of the corresponding omegasome. (D) HEK293 cells stably expressing GFP–DFCP1 and mCherry–Atg13 were transfected with CFP-LC3 for 24 hours, starved and imaged live. Two representative frames corresponding to different time points from the beginning of filming are shown. Arrows point to structures that are marked with all three proteins. (E) Representative montage illustrating an autophagosome formation sequence. Frames were captured every 10 seconds. White arrowheads indicate the emergence of the Atg13 particle and the omegasome. Yellow arrowheads indicate the structures that are marked with all three proteins. White arrows indicate the structures after the exit of Atg13. Yellow arrows point to LC3-positive membrane budding off the omegasome. The drawing illustrates the spatial relationship between the omegasome and the autophagosome of the corresponding frame. Scale bars: ~10 μm (A,D); ~1 μm (B,E).

ER is the most frequent proximal membrane to new autophagosomes

The very clear response to starvation of cells expressing GFP–Atg13, and the certainty by which newly formed puncta could be identified by spinning disk confocal microscopy, prompted us to systematically examine the spatial relationship of early autophagic structures to various cellular membranes. In all, we examined over 180 biogenesis events. We found that emerging autophagic puncta are distinct from the strands of the ER, but they remain constantly bound to the ER during their biogenesis. In contrast, the nature of the association between these particles and mitochondria is less tight and a similar result holds for lysosomes. These findings are true even when downstream expansion of the early GFP–Atg13 structures is blocked by wortmannin, and are consistent with previous work (Itakura and Mizushima, 2010). Since the ULK1 complex is the earliest functional complex of the core autophagy machinery that targets the precursor structures of autophagosomes, its localization provides insight into the origin of the autophagosomal membrane and the mechanisms by which it might be delivered. The stable association between the particles of the ULK1 complex and ER implies that the ULK1 complex targets a membrane compartment that is connected to ER. We can imagine two alternative types of connection: membrane continuity or peripheral binding. Membrane continuity suggests that membrane can be provided to the expanding isolation membrane (IM) directly. In contrast, peripheral binding suggests that membrane can be provided to the IM indirectly, possibly employing machinery similar to the mitochondrial association ER membranes (MAMs) (Kornmann et al., 2009). The nature of the association between the ULK1-positive IM and mitochondria, the second candidate source of the autophagosomal membrane (Hailey et al., 2010), is transient, precluding that membrane continuity between these organelles exists, at least as a general phenomenon. Therefore, membrane transport should be indirect, through vesicular carriers or membrane contact sites. Indeed, the MAMs could offer a plausible mechanism to transport membrane, either directly from mitochondria to autophagosomes or indirectly through ER,

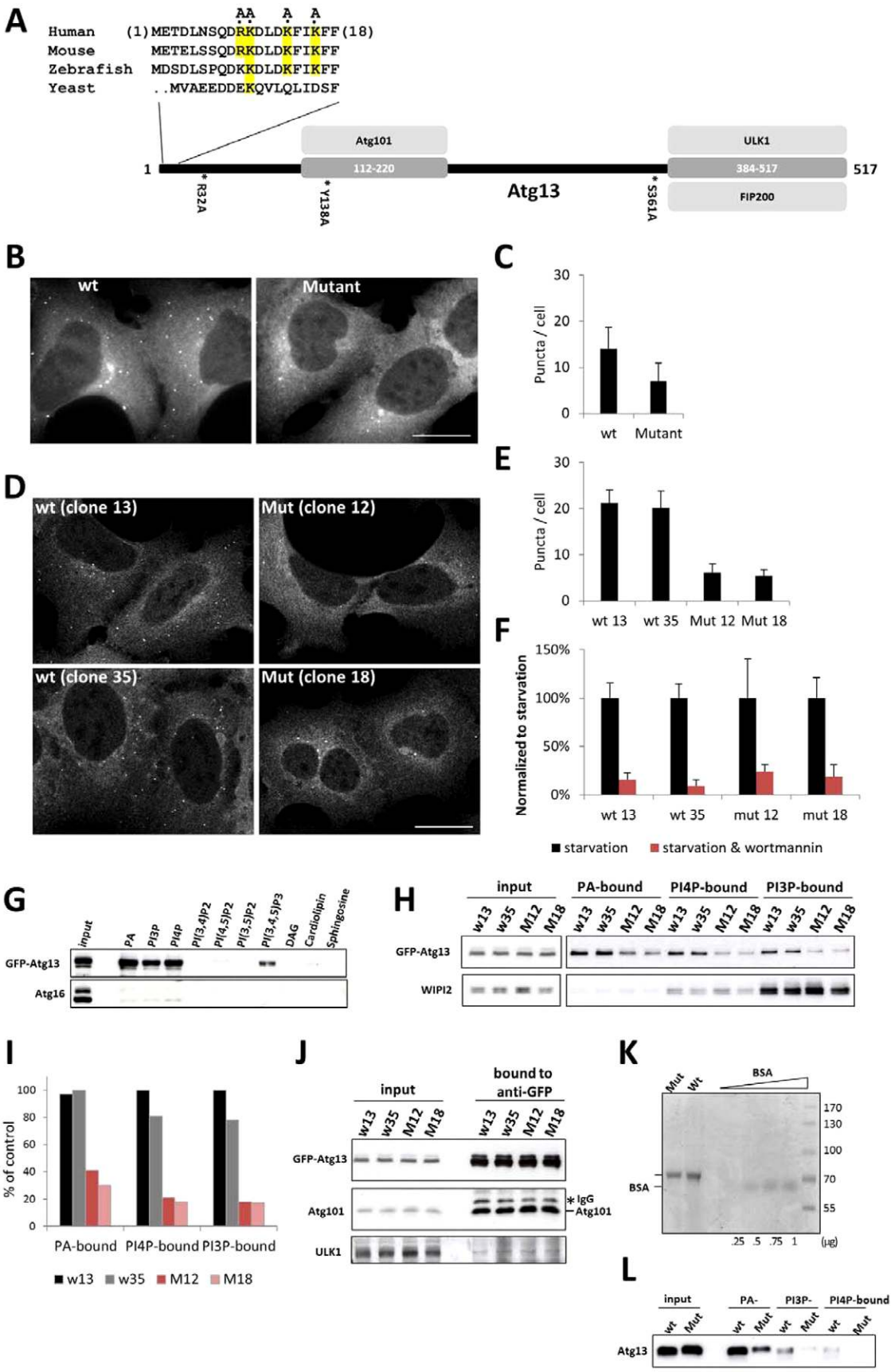

Fig. 5. See next page for legend.

consistent with the fact that the ER is always in close proximity (Hamasaki et al., 2013). Finally, we can envision that membrane originating from the third candidate source, the plasma membrane, could be transported to autophagosomes through endocytic vesicles [such as those containing the ULK1 protein (Longatti and Tooze, 2009)] that fuse with the IM, in agreement with two recent studies (Moreau et al., 2011; Nair et al., 2011).

Relationship of the ULK1 complex with omegasomes and with the isolation membrane

Almost simultaneously to its translocation to ER, the ULK1 complex associates with one DFCP1-positive omegasome, within which one IM first appears. The nature of this association is not known. One plausible mode of interaction *in trans* is that the ULK1 punctum may comprise a cluster of vesicles instead of being a single structure [such as the ULK1-containing recycling endosomes shown by Longatti et al. (Longatti and Tooze, 2009)], but we cannot discern any such collection of vesicles. Our favoured interaction mode is that the particles of the ULK1 complex consist of the same membranes as the corresponding omegasomes and IMs. The ULK1 complex could target one or both sides of the flat IM, and the DFCP1 ring would mark the boundaries of the LC3-positive IM. This spatial arrangement would allow ULK1 to access and bind LC3, something that has been recently reported (Kraft et al., 2012). The driving force for the omegasome–ULK1 interaction may involve multiple proteins. It is clear from a number of studies that the ULK1 complex must have some affinity for membranes (Chan et al., 2009), especially those related to the ER (Chan et al., 2009; Itakura and Mizushima, 2010), since upon the induction of autophagy the early ULK1-positive puncta are found associated with these membranes. In yeast, where a partial crystal structure exists, it appears that a region of Atg1 (Atg1 is equivalent to the mammalian ULK proteins) contains a domain that responds to membrane curvature (Ragusa et al., 2012), and an equivalent region in ULK1 has also been reported (Chan et al., 2009). Based on our data, a second region that may allow interaction of the ULK1 complex with membranes is at the N-terminus of Atg13 and it depends on a cluster of positively charged residues. The dominant-negative effect of the mutations at the N-terminus of Atg13 on autophagy suggests that Atg13 may have an essential function in the translocation of the entire ULK1 complex to puncta, which would lead to autophagy induction. Indeed, we have shown that, in Atg13 knockout MEFs, the wt GFP–Atg13 could rescue the formation of WIPI2 and Atg16 puncta in contrast to the mutant. This finding suggests that the ULK1 complex requires the affinity of Atg13 for membranes in order to stimulate autophagosome formation.

We cannot at this point reach a conclusion as to the lipid preference of Atg13. For protein obtained from mammalian lysates, similar preference for PA, PtdIns3*P* and PtdIns4*P* was detected, whereas protein isolated from bacteria showed a stronger preference for PA, followed by PtdIns3*P* and lastly for PtdIns4*P*. In the absence of a crystal structure, the safest hypothesis is that Atg13 has affinity for negatively charged membranes (the three preferred lipids would all be the simplest representative of such a membrane), somewhat analogous to the situation with Atg14, another early autophagy protein driving the Vps34 complex to the ER (Fan et al., 2011; Matsunaga et al., 2010).

A model of autophagosome formation incorporating ULK1 and omegasomes

Aligning the findings of this study with the literature, we propose the following model for autophagosome formation through an omegasome intermediate (Fig. 7). Once the mTOR complex is inactivated, the ULK1 complex becomes activated and translocates to the precursors of omegasomes, which are associated with the ER. On the ER, the ULK1 complex contributes to the activation of the Vps34 complex synthesising PtdIns3*P* for the nucleation of omegasomes. PtdIns3*P* further stimulates the recruitment of the ULK1 complex, creating a positive feedback loop that sustains the activation of additional molecules of the Vps34 complex. The continuous synthesis of PtdIns3*P* drives the formation and expansion of the DFCP1-positive omegasomes and leads to the recruitment of downstream components. Such downstream components are the WIPI proteins and perhaps Atg9 vesicles, which are followed by the assembly of the ubiquitin-like conjugation systems and the lipidation of LC3. Having a system in place for the localised lipidation of LC3 will further induce the expansion of the IM, while the ULK1 complex remains attached to the IM. When this machinery has achieved expansion of the mixed membrane to its maximum size, the ULK1 complex dissociates from the IM, the omegasome starts collapsing, and the LC3-positive IM buds off from the omegasome ring. At the latest stage, the omegasome ring closes, while the mature autophagosome is released and eventually it fuses with the lysosomes. The mechanism by which the ULK1

Fig. 5. Atg13 targeting to puncta is facilitated by its affinity for acidic phospholipids. (A) Atg13 primary sequence, illustrating the amino acid stretches that are necessary for binding to its partners (Jung et al., 2009; Mercer et al., 2009). One arginine and three lysines (highlighted in the sequence) were mutated to alanines. Asterisks indicate other point mutations of conserved residues of Atg13 that did not affect localization. A sequence alignment of these residues in human, mouse, zebrafish and yeast is shown at the top. (B) HEK293 cells stably expressing the mutant Atg13 were starved and their response was compared with the wt GFP–Atg13 clone. Representative images are shown. (C) The number of GFP–Atg13 puncta per cell in B for 20 different fields, containing 5–10 cells each (values are means ± s.d.). (D) Translocation of the mutant Atg13 to puncta under starvation for stable clones. (E) The number of GFP–Atg13 puncta per cell from D, for five different fields containing 15–30 cells each (values are means ± s.d.). (F) Clones of HEK293 cells stably expressing the mutant Atg13 were starved in the absence or presence of wortmannin, and their response was compared with the wt GFP–Atg13 clones. Values are means ± s.d. of the number of GFP–Atg13 puncta per cell, normalized to the response in the absence of wortmannin, for five different fields, containing 15–30 cells each. (G) Lysates from HEK293 cells stably expressing GFP–Atg13 (clone 35) were incubated with a panel of beads coated with lipids as shown, eluted with SDS-PAGE sample buffer, and the recovered proteins were assessed by western blotting using antibodies against GFP and Atg16. (H) Lysates from clones in D were incubated with beads coated with PA, PtdIns4*P* (PI4P) and PtdIns3*P*, and the recovered proteins were immunoblotted using antibodies against GFP and WIPI2. (I) Western blots from H were quantified with ImageJ, and values of recovered wt and mutant GFP–Atg13 normalized to the control are shown. (J) Wt and mutant Atg13 in lysates from H were immunoprecipitated with antibody against GFP, and blotted using antibodies against GFP, Atg101 and ULK1. Inputs are the same as for H and the gel is simply duplicated. (K) Recombinant wt and mutant His–Atg13 were purified from *E. coli*, and the eluates were run in an SDS-PAGE gel and stained with Coomassie Blue. BSA was run to quantify the amounts of purified proteins. (L) Equal amounts of wt and mutant His-Atg13 from K were incubated with lipid-coated beads as in H, and recovered Atg13 was immunoblotted using antibody against Atg13. Scale bars: ~10 μm.

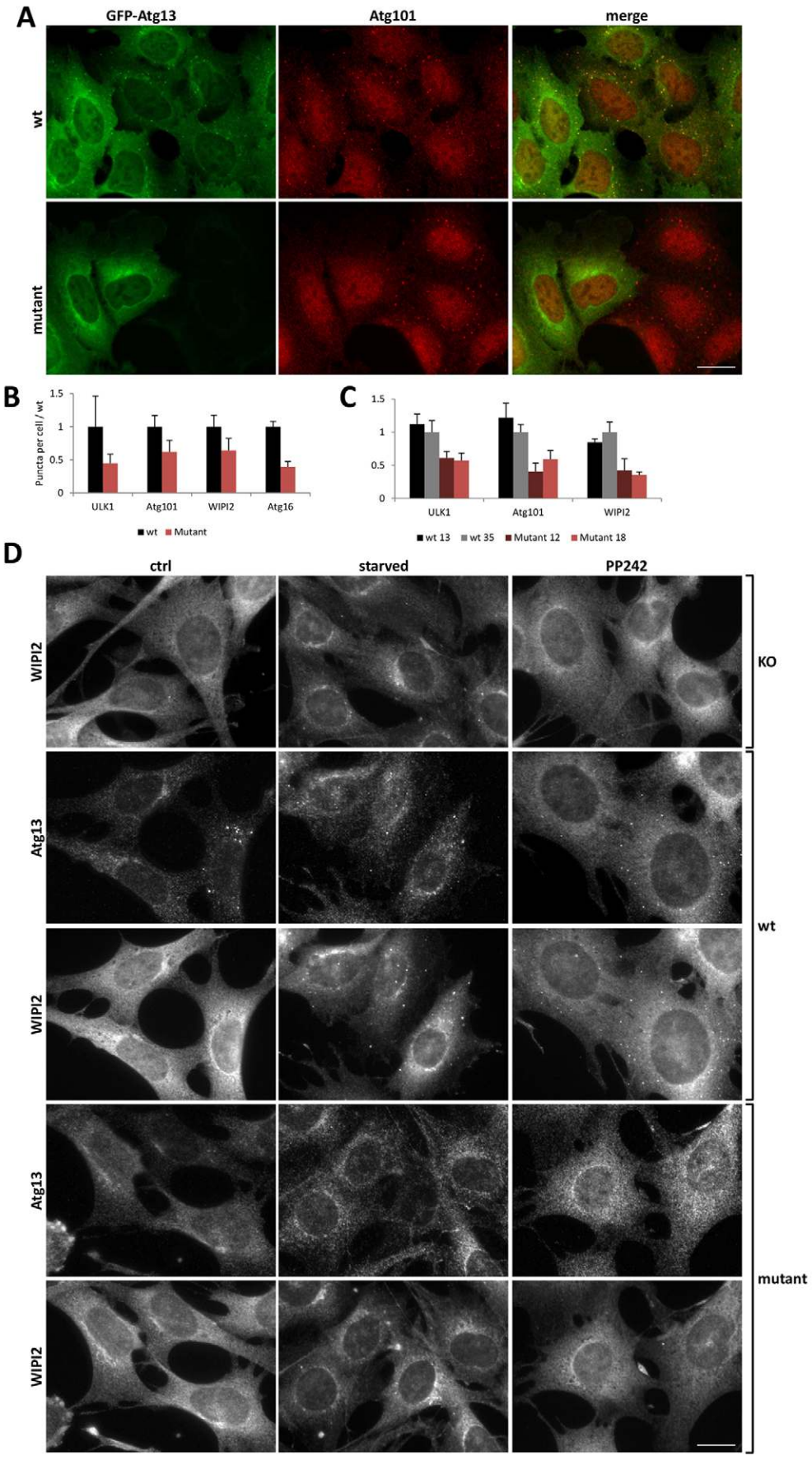

Fig. 6. Expression of mutant Atg13 inhibits formation of puncta by early autophagy markers. (A) HEK293 cells stably expressing the mutant Atg13 at different levels were starved, immunolabelled with antibodies against ULK1, Atg101, WIPI2 and Atg16, and their response was compared with the wt GFP–Atg13 clone. Representative images for Atg101 labelling are shown. (B) of The number of ULK1, Atg101, WIPI2 and Atg16 puncta normalized to the corresponding number of puncta of the wt clone 35, for five different fields containing 5–10 cells each (values are means ± s.d.). (C) Clonal cell lines stably expressing the wt and mutant GFP–Atg13 from Fig. 5D were starved and immunolabelled with antibodies against ULK1, Atg101 and WIPI2. Values are means ± s.d. of the number of ULK1, Atg101 and WIPI2 puncta normalized to the corresponding number of puncta of the wt clone 35, for five different fields containing 15–30 cells each. (D) Atg13 knockout (KO) MEFs stably expressing wt or mutant GFP–Atg13, were starved or treated with PP242 for 1 hour and immunolabelled for GFP and endogenous WIPI2. Scale bars: ~10 μm.

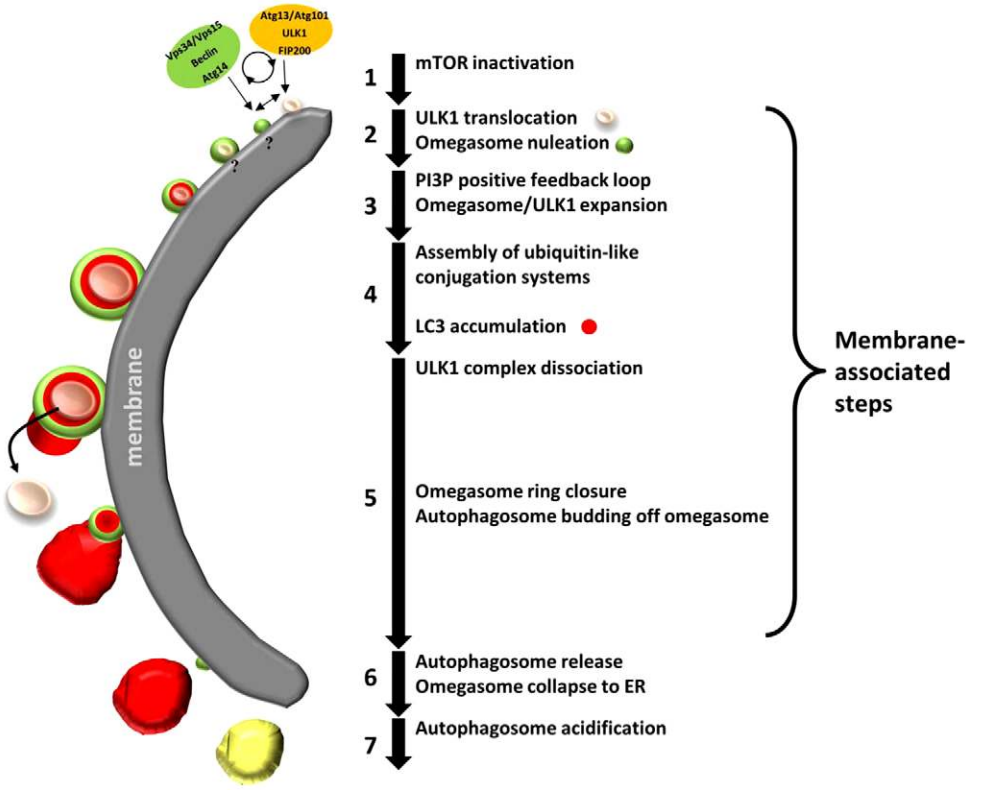

Fig. 7. Model of autophagosome formation through an omegasome intermediate. The autophagosome formation cascade begins in the cytosol with a signal that inactivates mTOR (step 1). Then, the activated ULK1 complex translocates to ER, where it activates the Vps34 complex, inducing the synthesis of PtdIns3*P* (PI3P) and nucleating a new omegasome (step 2). Sustained synthesis of PtdIns3*P* creates of positive feedback loop that reinforces the recruitment of additional molecules of the ULK1 complex on the IM, and stimulates the expansion of the omegasome (step 3). At the same time, the ubiquitin-like conjugation systems assemble on the IM where they begin to lipidate LC3 molecules, further inducing the expansion of the IM (step 4). Next, the ULK1 complex dissociates from the IM, the omegasome ring begins to close, and LC3-positive membrane buds off of the omegasome ring (step 5). Finally, the omegasome collapses back to ER, the autophagosome is released (step 6) and eventually its lumen becomes acidic and fuses with the lysosomes for the degradation of its contents (step 7).

complex dissociates from the early membranes before autophagosome completion is unknown. One possibility is that inhibition of PtdIns3*P* synthesis [or activation of its degradation by Jumpy (Vergne et al., 2009) or other PtdIns3*P* phosphatases that might localise on the IM (Taguchi-Atarashi et al., 2010)] might break the positive feedback loop that allows the complex to be stabilised on membranes. Alternatively, a phosphorylation–dephosphorylation on the ULK1 complex mechanism might be at play. This interesting question will be explored in future work.

Materials and Methods

All chemicals were obtained from Sigma-Aldrich unless otherwise stated.

Antibodies

The antibodies used were: rabbit anti-ULK1 (Santa Cruz), rabbit anti-phospho-ULK1 (Ser757) (Cell Signaling Technology), rabbit anti-Atg13 (Sigma), mouse anti-Atg13 (Millipore), rabbit anti-Atg101 (Sigma), mouse anti-WIPI2 (gift from S. Tooze, London Research Institute, London, UK), rabbit anti-Atg16 (MBLI), rabbit anti-Vps34 (Invitrogen), rabbit anti-beclin1 (Santa Cruz) and mouse anti-GFP (Roche).

Plasmids used in this work

pEGFP-C1-Atg13 [Addgene (Hosokawa et al., 2009)] was a gift of M. Wilson (Babraham Institute, Cambridge, UK). Site-directed mutagenesis to generate the point mutations within pEGFP-C1-Atg13(R10A K11A K15A K18A) was performed using standard PCR techniques. pCDNA4-TO-mCherry-Atg13 was used for the construction of the cell line stably expressing mCherry-Atg13. To obtain pCDNA4-TO-mCherry-Atg13, the Atg13 ORF was cleaved with *Bam*HI from the pEGFP-C1-Atg13 plasmid and was subcloned into the pmCherry-C1 vector (Clontech) for the construction of pmCherry-C1-Atg13. The mCherry-Atg13 cassette was then cleaved from pmCherry-C1-Atg13 with *Age*I–*Xba*I and subcloned into the pcDNA4-TO-mRFP-Vps34 (Axe et al., 2008), from which the mRFP-Vps34 cassette was removed with the same restriction enzymes. pmCherry-dgk1 was a gift of S. Siniossoglou (Cambridge Institute for Medical Research, Cambridge, UK). Lamp1-RFP plasmid was purchased from Addgene (Sherer et al., 2003). The plasmid for the expression of CFP–LC3 was a gift from T. Yoshimori (Department of Genetics, Osaka University Graduate School of Medicine, Osaka, Japan). pOPH10-Atg13 and pOPH10-Atg13(R10A K11A K15A K18A) plasmids were used for the expression of recombinant forms of His-tagged wt and mutant Atg13. For the construction of pOPH10-Atg13 and pOPH10-Atg13(R10A K11A K15A K18A) plasmids, wt and mutant Atg13 were amplified by PCR from the pEGFP-C1-Atg13 and pEGFP-C1-Atg13(R10A K11A K15A K18A) plasmids respectively, cleaved with *Nde*I–*Bam*HI and subcloned into pOPH10 vector (gift from M. Wilson, Babraham Institute, Cambridge, UK). For the construction of pBABE-Puro-GFP-Atg13 and pBABE-Puro-Atg13(R10A K11A K15A K18A) plasmids, the GFP-Atg13 cassette was cleaved with *Age*I–*Xba*I from the pCDNA4-TO-mCherry-Atg13 or pCDNA4-TO-mCherry-Atg13(R10A K11A K15A K18A) plasmid, filled in with T4 DNA polymerase and subcloned into the pBABE-Puro vector (Cell Biolabs) that was opened with *Bam*HI and filled-in with T4 DNA polymerase.

Cell culture, transfections, and generation of stable cell lines

HEK293 and mouse embryonic fibroblast (MEF) cell lines were grown in DME (Invitrogen) containing 100 U/µl penicillin and streptomycin (Invitrogen) and 10% fetal calf serum (Invitrogen). Stable GFP–Atg13-expressing cell lines were selected in 800 µg/ml geneticin (Invitrogen). Stable GFP–DFCP1- and mCherry–Atg13-expressing cell lines were selected in 800 µg/ml geneticin and 100 µg/ml zeocin. For establishment of MEFs stably expressing GFP-Atg13 and GFP-Atg13(R10A K11A K15A K18A), a Platinum-E Retroviral Packaging Cell Line (Cell Biolabs) was transfected with either pBABE-Puro-GFP-Atg13 or pBABE-Puro-Atg13(R10A K11A K15A K18A) plasmids, the retroviral supernatant was used to infect the MEFs, and cells were selected with 0.5 µg/ml puromycin. HEK293 cell lines were transfected using X-treme GENE 9 DNA Transfection Reagent (Roche Applied Science) according to the manufacturer's instructions.

siRNA

We used predesigned oligonucleotides from Thermo Fisher Scientific (SMARTpool) to reduce expression levels of beclin1. Cells were transfected using DharmaFECT 1 and examined 72 hours later.

Generation of *Atg13* knockout MEFs

Atg13 knockout (KO) MEFs were obtained from *Atg13gt/gt* mouse embryos, which were generated using an ES cell line DD0507 [obtained from the Sanger Institute Gene Trap Resources (SIGTR) through Mutant Mouse Regional Resource Centers) containing an insertion of a gene trap cassette in the *Atg13* gene, and immortalized with SV40 large T antigen using pEF321-T (T. K. and N. M., unpublished data).

Starvation of HEK293 cells, induction and inhibition of autophagy

For amino acid starvation, cells were washed three times with pre-warmed starvation medium (140 mM NaCl, 1 mM $CaCl_2$, 1 mM $MgCl_2$, 5 mM glucose, 1% BSA and 20 mM Hepes pH 7.4), before incubation with starvation medium. The duration of the starvation treatment varied between experiments, as indicated. mTOR was inhibited by the addition of 1 μM PP242 to the medium. PI 3-kinase was inhibited by the addition of 10 nM wortmannin to the medium. Duration of the treatments varied between experiments.

Immunofluorescence microscopy

Cells for immunofluorescence were grown on glass coverslips and fixed in 3.7% formaldehyde in 200 mM Hepes, pH 7.2. Staining for immunofluorescence and digital imaging was done as described previously (Manifava et al., 1999).

Binding of proteins to phospholipid-conjugated beads

HEK293 cells expressing the appropriate constructs were lysed in lysis buffer (50 mM Tris-HCl, pH 8.0, 50 mM KCl, 10 mM EDTA, 0.6 mM phenylmethylsulfonyl fluoride, 1 μg/ml trypsin inhibitor, and 0.5% Nonidet P-40) and centrifuged at 14,000 ***g*** to remove cell debris. Binding to phospholipid-coupled beads was done as described previously (Manifava et al., 2001).

Immunoprecipitations

Lysates from HEK293 cells stably expressing wt and mutant GFP–Atg13 that were prepared for the binding to phospholipids-conjugated beads were used for immunoprecipitation. GFP–Atg13 was immunoprecipitated with anti-GFP antibody (Roche).

Confocal imaging

Images were captured with an Olympus FV1000 confocal microscope using a 60× 1.4 NA objective (Olympus).

Quantitation of puncta

Quantification and determination of colocalization of puncta was performed using the Spots Detection function of Imaris software (Bitplane/Andor). The measurements were made on randomly selected fields of view.

Epifluorescence imaging

Images of fixed cells were acquired using a Zeiss Axio Imager D2 wide-field epifluorescence microscope equipped with a 63× 1.4 NA lens, AxioCam HR CCD camera (Zeiss) and HXP 120C metal halide light source (Zeiss).

Super-resolution microscopy

Super-resolution images were acquired using a Nikon N-SIM structured illumination microscope. Cells were cultured on high precision 18 mm glass coverslips (Marienfeld) and mounted in ProLong Gold (Invitrogen). The Nikon N-SIM system consisted of a Nikon Ti-E microscope, a Nikon structured illumination system using 488 nm laser light (for GFP) and 561 nm laser light (for DsRed), 100× 1.49 NA lens and an Andor iXon 897 camera. Nikon Elements software was used for image acquisition and super resolution image reconstruction.

Live-cell imaging

Two imaging systems were used to capture images of live cells. Confocal images were taken using a spinning disk confocal microscope (Andor Technology plc.); wide-field images were taken using a Cell^R imaging system (Olympus). For both systems, cells were plated onto 22 mm diameter glass coverslips (BDH) and transiently transfected with the relevant constructs, then individual coverslips were secured in an imaging chamber and 2 ml of cell medium or starvation medium added as indicated. The assembled imaging chamber was secured onto the microscope stage, and cells were maintained at 37℃ using a full enclosure incubation system (Solent Scientific). The Spinning Disk confocal was equipped with a Nikon Ti-E microscope, 100× 1.4 NA objective (Nikon), EM-CCD camera (Andor iXon 897), and laser to excite at 488 (GFP) and 561 nm (mRFP). Emission was collected using 497–547 nm (GFP) and 577–622 (DsRed) band-pass filters mounted in a Sutter filter wheel. A Z-stack of six planes with a 0.1 μm step between them was captured for each time point in order to increase the scanned cell volume and improve the resolution by deconvolving the videos. Hyper-stacks (stacks of six Z-stacks from each time point) were deconvolved using Huygens Professional (Scientific Volume Imaging), and converted to stacks of flat images by projecting each Z-stack using the 'Z Project' plugin of Fiji (Fiji Is Just ImageJ) Open Source software. The Cell^R imaging system was equipped with a 100× 1.4 NA objective (Olympus), Polychrome V monochromator (TILL Photonics) and a Hamamatsu Orca CCD camera. CFP, GFP and mRFP were excited at 425, 488 and 585 nm, respectively, typically using 10 nm bandwidth and 20% transmission. Bandpass filters at 467–500 nm, 505–545 nm, and 605–680 nm were used to collect fluorescent light from CFP, GFP and mRFP, respectively.

Analysis of live-cell imaging videos

Live-cell imaging videos were analysed with Fiji Open Source software. We define as an independent event all the frames that correspond to the formation and collapse of one GFP–Atg13 particle, starting and finishing with the frames in which the fluorescence of the GFP–Atg13 particle is emerging clearly above the fluorescence of the cytosolic GFP–Atg13 (e.g. Fig. 4C). Frames corresponding to time points before the beginning or after the end of a particular event were carefully scanned, and events corresponding to particles moving out of focus and then back in were excluded from the analysis. For the analysis of the distance between GFP–Atg13 and the different organelles, lines were drawn in Fiji, the fluorescence intensities for the green and red channels were analysed using the 'Colour Profiler' plugin, and the distance in pixels between the peaks was measured.

Purification of recombinant proteins

pOPH10-Atg13 and pOPH10-Atg13(R10A K11A K15A K18A) plasmids for the expression of wt and mutant form of His-tagged Atg13 were used to transform C41 DE3 bacteria. Overnight pre-cultures were diluted and grown at 37℃ to OD_{600}=0.6, shifted at 16℃, and expression of Atg13 was induced for 24 hours with 0.1 mM IPTG. Cells were pelleted, washed with PBS and flash-frozen with liquid nitrogen. Bacterial pellets were resuspended in lysis buffer (20 mM Tris–HCl pH 8.0, 150 mM NaCl, 1% Triton X-100, 10 mM Imidazole), were lysed by sonication, and unbroken cells and debris were removed by centrifugation at 30,000 ***g*** for 30 minutes. The cleared lysates were incubated with nickel beads (His-select; Sigma-Aldrich) for 1 hour at 4℃, washed twice with lysis buffer, and the His-tagged Atg13 was eluted with 250 mM Imidazole. Eluates were concentrated and the buffer was changed to storage buffer (20 mM Tris-HCl pH 8.0, 150 mM NaCl, 10% glycerol).

Acknowledgements

We thank our colleagues listed in Materials and Methods for their generous sharing of various antibodies and plasmids. We thank Dr Sumio Sugano (the University of Tokyo) for the pEF321-T plasmid. We thank Roger Williams for pointing out potential membrane interacting sites in Atg13, and Len Stephens, Phill Hawkins and Sharon Tooze for many useful discussions.

Author contributions

E.K. and N.T.K. designed research; E.K., E.S., M.M., and S.A.W. performed research; E.K., E.S., S.A.W. and N.T.K. analyzed data; T.K. and N.M. contributed data and reagents; E.K. and N.T.K. wrote the paper.

Funding

This work is supported by the Biotechnology and Biological Sciences Research Council [grant number BB/H000631/1 to N.T.K.]; and a science policy committee grant from the Babraham Institute, Cambridge [grant number 2301-R1600-C0341 to N.T.K.].

Supplementary material available online at
http://jcs.biologists.org/lookup/suppl/doi:10.1242/jcs.132415/-/DC1

References

Axe, E. L., Walker, S. A., Manifava, M., Chandra, P., Roderick, H. L., Habermann, A., Griffiths, G. and Ktistakis, N. T. (2008). Autophagosome formation from membrane compartments enriched in phosphatidylinositol 3-phosphate and dynamically connected to the endoplasmic reticulum. *J. Cell Biol.* **182**, 685-701.

Bodemann, B. O., Orvedahl, A., Cheng, T., Ram, R. R., Ou, Y.-H., Formstecher, E., Maiti, M., Hazelett, C. C., Wauson, E. M., Balakireva, M. et al. (2011). RalB and the exocyst mediate the cellular starvation response by direct activation of autophagosome assembly. *Cell* **144**, 253-267.

Burman, C. and Ktistakis, N. T. (2010). Autophagosome formation in mammalian cells. *Semin. Immunopathol.* **32**, 397-413.

Chan, E. Y. W., Longatti, A., McKnight, N. C. and Tooze, S. A. (2009). Kinase-inactivated ULK proteins inhibit autophagy via their conserved C-terminal domains using an Atg13-independent mechanism. *Mol. Cell. Biol.* **29**, 157-171.

Chang, Y. Y. and Neufeld, T. P. (2009). An Atg1/Atg13 complex with multiple roles in TOR-mediated autophagy regulation. *Mol. Biol. Cell* **20**, 2004-2014.

Conway, S. J., Gardiner, J., Grove, S. J. A., Johns, M. K., Lim, Z.-Y., Painter, G. F., Robinson, D. E. J. E., Schieber, C., Thuring, J. W., Wong, L. S.-M. et al. (2010). Synthesis and biological evaluation of phosphatidylinositol phosphate affinity probes. *Org. Biomol. Chem.* **8**, 66-76.

Delon, C., Manifava, M., Wood, E., Thompson, D., Krugmann, S., Pyne, S. and Ktistakis, N. T. (2004). Sphingosine kinase 1 is an intracellular effector of phosphatidic acid. *J. Biol. Chem.* **279**, 44763-44774.

Di Bartolomeo, S., Corazzari, M., Nazio, F., Oliverio, S., Lisi, G., Antonioli, M., Pagliarini, V., Matteoni, S., Fuoco, C., Giunta, L. et al. (2010). The dynamic interaction of AMBRA1 with the dynein motor complex regulates mammalian autophagy. *J. Cell Biol.* **191**, 155-168.

Fan, W., Nassiri, A. and Zhong, Q. (2011). Autophagosome targeting and membrane curvature sensing by Barkor/Atg14(L). *Proc. Natl. Acad. Sci. USA* **108**, 7769-7774.

Ganley, I. G., Lam, H., Wang, J., Ding, X., Chen, S. and Jiang, X. (2009). ULK1.ATG13.FIP200 complex mediates mTOR signaling and is essential for autophagy. *J. Biol. Chem.* **284**, 12297-12305.

Geng, J., Nair, U., Yasumura-Yorimitsu, K. and Klionsky, D. J. (2010). Post-Golgi Sec proteins are required for autophagy in Saccharomyces cerevisiae. *Mol. Biol. Cell* **21**, 2257-2269.

Hailey, D. W., Rambold, A. S., Satpute-Krishnan, P., Mitra, K., Sougrat, R., Kim, P. K. and Lippincott-Schwartz, J. (2010). Mitochondria supply membranes for autophagosome biogenesis during starvation. *Cell* **141**, 656-667.

Hamasaki, M., Furuta, N., Matsuda, A., Nezu, A., Yamamoto, A., Fujita, N., Oomori, H., Noda, T., Haraguchi, T., Hiraoka, Y. et al. (2013). Autophagosomes form at ER-mitochondria contact sites. *Nature* **495**, 389-393.

Hayashi-Nishino, M., Fujita, N., Noda, T., Yamaguchi, A., Yoshimori, T. and Yamamoto, A. (2009). A subdomain of the endoplasmic reticulum forms a cradle for autophagosome formation. *Nat. Cell Biol.* **11**, 1433-1437.

Hosokawa, N., Hara, T., Kaizuka, T., Kishi, C., Takamura, A., Miura, Y., Iemura, S., Natsume, T., Takehana, K., Yamada, N. et al. (2009). Nutrient-dependent mTORC1 association with the ULK1-Atg13-FIP200 complex required for autophagy. *Mol. Biol. Cell* **20**, 1981-1991.

Inoue, Y. and Klionsky, D. J. (2010). Regulation of macroautophagy in Saccharomyces cerevisiae. *Semin. Cell Dev. Biol.* **21**, 664-670.

Itakura, E. and Mizushima, N. (2010). Characterization of autophagosome formation site by a hierarchical analysis of mammalian Atg proteins. *Autophagy* **6**, 764-776.

Jung, C. H., Jun, C. B., Ro, S.-H., Kim, Y. M., Otto, N. M., Cao, J., Kundu, M. and Kim, D.-H. (2009). ULK-Atg13-FIP200 complexes mediate mTOR signaling to the autophagy machinery. *Mol. Biol. Cell* **20**, 1992-2003.

Klionsky, D. J., Abdalla, F. C., Abeliovich, H., Abraham, R. T., Acevedo-Arozena, A., Adeli, K., Agholme, L., Agnello, M., Agostinis, P., Aguirre-Ghiso, J. A. et al. (2012). Guidelines for the use and interpretation of assays for monitoring autophagy. *Autophagy* **8**, 445-544.

Kornmann, B., Currie, E., Collins, S. R., Schuldiner, M., Nunnari, J., Weissman, J. S. and Walter, P. (2009). An ER-mitochondria tethering complex revealed by a synthetic biology screen. *Science* **325**, 477-481.

Kraft, C., Kijanska, M., Kalie, E., Siergiejuk, E., Lee, S. S., Semplicio, G., Stoffel, I., Brezovich, A., Verma, M., Hansmann, I. et al. (2012). Binding of the Atg1/ULK1 kinase to the ubiquitin-like protein Atg8 regulates autophagy. *EMBO J.* **31**, 3691-3703.

Krugmann, S., Anderson, K. E., Ridley, S. H., Risso, N., McGregor, A., Coadwell, J., Davidson, K., Eguinoa, A., Ellson, C. D., Lipp, P. et al. (2002). Identification of ARAP3, a novel PI3K effector regulating both Arf and Rho GTPases, by selective capture on phosphoinositide affinity matrices. *Mol. Cell* **9**, 95-108.

Longatti, A. and Tooze, S. A. (2009). Vesicular trafficking and autophagosome formation. *Cell Death Differ.* **16**, 956-965.

Lu, Q., Yang, P., Huang, X., Hu, W., Guo, B., Wu, F., Lin, L., Kovács, A. L., Yu, L. and Zhang, H. (2011). The WD40 repeat PtdIns(3)P-binding protein EPG-6 regulates progression of omegasomes to autophagosomes. *Dev. Cell* **21**, 343-357.

Manifava, M., Sugars, J. and Ktistakis, N. T. (1999). Modification of catalytically active phospholipase D1 with fatty acid in vivo. *J. Biol. Chem.* **274**, 1072-1077.

Manifava, M., Thuring, J. W., Lim, Z. Y., Packman, L., Holmes, A. B. and Ktistakis, N. T. (2001). Differential binding of traffic-related proteins to phosphatidic acid- or phosphatidylinositol (4,5)- bisphosphate-coupled affinity reagents. *J. Biol. Chem.* **276**, 8987-8994.

Matsunaga, K., Morita, E., Saitoh, T., Akira, S., Ktistakis, N. T., Izumi, T., Noda, T. and Yoshimori, T. (2010). Autophagy requires endoplasmic reticulum targeting of the PI3-kinase complex via Atg14L. *J. Cell Biol.* **190**, 511-521.

Mercer, C. A., Kaliappan, A. and Dennis, P. B. (2009). A novel, human Atg13 binding protein, Atg101, interacts with ULK1 and is essential for macroautophagy. *Autophagy* **5**, 649-662.

Mizushima, N. and Komatsu, M. (2011). Autophagy: renovation of cells and tissues. *Cell* **147**, 728-741.

Mizushima, N., Yoshimori, T. and Ohsumi, Y. (2011). The role of Atg proteins in autophagosome formation. *Annu. Rev. Cell Dev. Biol.* **27**, 107-132.

Moreau, K., Ravikumar, B., Renna, M., Puri, C. and Rubinsztein, D. C. (2011). Autophagosome precursor maturation requires homotypic fusion. *Cell* **146**, 303-317.

Nair, U., Jotwani, A., Geng, J., Gammoh, N., Richerson, D., Yen, W.-L., Griffith, J., Nag, S., Wang, K., Moss, T. et al. (2011). SNARE proteins are required for macroautophagy. *Cell* **146**, 290-302.

Orsi, A., Razi, M., Dooley, H. C., Robinson, D., Weston, A. E., Collinson, L. M. and Tooze, S. A. (2012). Dynamic and transient interactions of Atg9 with autophagosomes, but not membrane integration, are required for autophagy. *Mol. Biol. Cell* **23**, 1860-1873.

Polson, H. E. J. J., de Lartigue, J., Rigden, D. J., Reedijk, M., Urbé, S., Clague, M. J. and Tooze, S. A. (2010). Mammalian Atg18 (WIPI2) localizes to omegasome-anchored phagophores and positively regulates LC3 lipidation. *Autophagy* **6**, 506-522.

Proikas-Cezanne, T., Waddell, S., Gaugel, A., Frickey, T., Lupas, A. and Nordheim, A. (2004). WIPI-1alpha (WIPI49), a member of the novel 7-bladed WIPI protein family, is aberrantly expressed in human cancer and is linked to starvation-induced autophagy. *Oncogene* **23**, 9314-9325.

Rabinowitz, J. D. and White, E. (2010). Autophagy and metabolism. *Science* **330**, 1344-1348.

Ragusa, M. J. J., Stanley, R. E. E. and Hurley, J. H. H. (2012). Architecture of the Atg17 complex as a scaffold for autophagosome biogenesis. *Cell* **151**, 1501-1512.

Ravikumar, B., Moreau, K., Jahreiss, L., Puri, C. and Rubinsztein, D. C. (2010). Plasma membrane contributes to the formation of pre-autophagosomal structures. *Nat. Cell Biol.* **12**, 747-757.

Ridley, S. H., Ktistakis, N., Davidson, K., Anderson, K. E., Manifava, M., Ellson, C. D., Lipp, P., Bootman, M., Coadwell, J., Nazarian, A. et al. (2001). FENS-1 and DFCP1 are FYVE domain-containing proteins with distinct functions in the endosomal and Golgi compartments. *J. Cell Sci.* **114**, 3991-4000.

Rubinsztein, D. C., Shpilka, T. and Elazar, Z. (2012). Mechanisms of autophagosome biogenesis. *Curr. Biol.* **22**, R29-R34.

Sherer, N. M., Lehmann, M. J., Jimenez-Soto, L. F., Ingmundson, A., Horner, S. M., Cicchetti, G., Allen, P. G., Pypaert, M., Cunningham, J. M. and Mothes, W. (2003). Visualization of retroviral replication in living cells reveals budding into multivesicular bodies. *Traffic* **4**, 785-801.

Sridhar, S., Botbol, Y., Macian, F. and Cuervo, A. M. (2012). Autophagy and disease: always two sides to a problem. *J. Pathol.* **226**, 255-273.

Suzuki, K. and Ohsumi, Y. (2010). Current knowledge of the pre-autophagosomal structure (PAS). *FEBS Lett.* **584**, 1280-1286.

Taguchi-Atarashi, N., Hamasaki, M., Matsunaga, K., Omori, H., Ktistakis, N. T., Yoshimori, T. and Noda, T. (2010). Modulation of local PtdIns3P levels by the PI phosphatase MTMR3 regulates constitutive autophagy. *Traffic* **11**, 468-478.

Tooze, S. A. and Yoshimori, T. (2010). The origin of the autophagosomal membrane. *Nat. Cell Biol.* **12**, 831-835.

Vergne, I., Roberts, E., Elmaoued, R. A., Tosch, V., Delgado, M. A., Proikas-Cezanne, T., Laporte, J. and Deretic, V. (2009). Control of autophagy initiation by phosphoinositide 3-phosphatase Jumpy. *EMBO J.* **28**, 2244-2258.

Yang, Z. and Klionsky, D. J. (2010). Mammalian autophagy: core molecular machinery and signaling regulation. *Curr. Opin. Cell Biol.* **22**, 124-131.

Ylä-Anttila, P., Vihinen, H., Jokitalo, E. and Eskelinen, E.-L. (2009). 3D tomography reveals connections between the phagophore and endoplasmic reticulum. *Autophagy* **5**, 1180-1185.